Title

In Situ Volumetric Imaging and Analysis of FRESH 3D Bioprinted Constructs Using Optical Coherence Tomography

Authors

Joshua W. Tashman[1*], Daniel J. Shiwarski[1*], Alexander Ruesch[1], Frederick Lanni[2], Jana M. Kainerstorfer[1], Adam W. Feinberg[1,3]

[1]Department of Biomedical Engineering, Carnegie Mellon University, Pittsburgh, PA, 15213

[2]Department of Biological Sciences, Carnegie Mellon University, Pittsburgh, PA, 15213

[3]Department of Materials Science & Engineering, Carnegie Mellon University, Pittsburgh, PA, 15213

*These authors contributed equally: Joshua W. Tashman, Daniel J. Shiwarski.

Abstract

As 3D bioprinting has grown as a fabrication technology, so too has the need for improved analytical methods to characterize these engineered constructs. This is especially challenging for soft tissues composed of hydrogels and cells as these materials readily deform, posing a barrier when trying to assess print fidelity and other properties non-destructively. Indeed, given the importance of structure-function relationships in most tissue types, establishing that the 3D architecture of the bioprinted construct matches its intended anatomic design is critical. Here we report development of a multimaterial bioprinting platform with integrated optical coherence tomography (OCT) for in situ volumetric imaging, error detection, and 3D reconstruction. While generally applicable to extrusion-based 3D bioprinting, we also report improvements to the Freeform Reversible Embedding of Suspended Hydrogels (FRESH) bioprinting process through new collagen bioink compositions, support bath optical clearing, and machine pathing. This enables high-fidelity 3D volumetric imaging with micron scale resolution over centimeter length scales, the ability to detect a range of print defect types within a 3D volume, and real-time imaging of the printing process at each print layer. These advances provide FRESH and other extrusion-based 3D bioprinting approaches with a comprehensive methodology for quality assessment that has been absent in the field to date, paving the way for translation of these engineered tissues to the clinic and ultimately to achieving regulatory approval.

Teaser

Transparent FRESH support bath enables in situ 3D volumetric imaging and validation of patient-derived tissue constructs.

Introduction:

As the demand for donor tissue and organs continues to outpace the supply, clinicians are turning to regenerative medicine and tissue engineering strategies to create tissue *de novo*. 3D bioprinting has emerged as a way to build these tissues using robotic control to precisely pattern cells and biological hydrogels in a layer-by-layer process. However, this technology has been slowed by the difficulty of printing these soft, deformable materials into complex 3D architectures that recapitulate anatomic structure from the micro to macro length scale, and by the lack of a quantitative approach to verify print fidelity. Embedded 3D bioprinting, such as Freeform Reversible Embedding of Suspended Hydrogels (FRESH), addresses thischallenge by providing a sacrificial support that prevents tissue deformation during bioprinting to produce highly relevant constructs such as heart valves, cardiac tissue scaffolds, and perfusable vascular networks (*1*–*4*). These sophisticated bioprinted constructs could prove very useful as clinical diagnostic tools or direct tissue replacements (*2*, *3*, *5*–*7*). However, for successful translation into an approved therapy, assessment of the manufactured product becomes increasingly important. To continue to move bioprinting techniques such as FRESH towards clinical application 1) the printing capabilities must be improved to allow for high-fidelity reproduction of patient-specific organic shapes 2) the accuracy and precision of bioprinted tissues must be directly assessed and quantified and 3) quality control of geometric fidelity and error detection utilizing feedback from in-process measurements of the tissue during printing must be implemented. In fact, for a medical device to be approved by the U.S. Food and Drug Administration, process validation and performance qualification, such as in-process monitoring during manufacturing, is required to ensure

a product consistently meets predetermined specifications (FDA e-CFR §820.70, §820.72, §820.75).

For most manufacturing, in-process monitoring can be performed using light-based camera systems or machine vision, and does not require true 3D reconstruction for validation (*8*). However, for FRESH, implementing these traditional approaches is challenging. The gelatin microparticle support bath that is essential for the FRESH printing process is opaque and highly light scattering (*1*, *2*). Micro Computed Tomography (μCT) has been performed on FRESH printed samples to produce 3D reconstructions after they have been removed from the support bath (*2*), but this process requires sample fixation and embedding into an agarose solution which limits its use as a therapeutic device after imaging. 3D fluorescence imaging can be non-destructive and resolve micron scale features, but is limited by slow acquisition speeds and small volumetric imaging (constructs less than 1 mm in thickness). An ideal inspection solution would need to have a large imaging depth and field of view, a fast volumetric acquisition speed, would need to resolve features from the micron to centimeter scale, and would be non-destructive to the sample. A potential imaging modality that fulfills these requirements is optical coherence tomography (OCT).

There are several types of OCT, but we have chosen swept-source OCT for its large penetration depth due to a long wavelength (1300 nm) light source and fast scanning speed of 100 kHz which can image 1 cm^3 3D volumes in less than 5 minutes (Thorlabs Vega) (*9*). In general, OCT works by splitting a coherent light source between two light paths, a reference and sample arm. As the light returns from each respective light path the interaction of the waveforms produces either constructive (displayed as a

bright object) or destructive interference (displayed as a dark object). Therefore, if the sample is highly reflective it will appear as a bright object of high signal intensity, and if there is no reflection and the sample absorbs the light the signal will be low and appear dark. OCT has been a valuable tool for clinical imaging in ophthalmology of the retina and cornea (*10*–*12*), creating 3D angiograms (*13*, *14*), and even monitoring fabrication and quality of electronic devices (*15*, *16*). More recently, the use of OCT has emerged in the 3D printing space to monitor print quality for simple process feedback control, and to image collagen, PEG, and 3D printed hydrogel scaffolds after printing (*17*–*22*). While these reports demonstrate the advantages of using OCT to characterize a final printed scaffold, there remains a need to implement an in-process monitoring, quality control, and feedback system, such as OCT, into high performance 3D bioprinters to facilitate the transition of bioprinted tissues and organs into an FDA approved therapy.

Here we developed a complete in-process 3D imaging platform for bioprinting consisting of a custom-built dual extruder 3D bioprinter with an integrated OCT system to perform real-time imaging during FRESH printing. In addition to developing the custom hardware, we enhanced the OCT contrast of our collagen I bioink, developed a method to image prints larger than the maximum imaging depth (>8.3 mm), and created a transparent support bath to address the problem of FRESH gelatin microparticle support bath opacity. Finally, we demonstrate that OCT imaging can be performed live during printing, intermittently between print layers, or following print completion. Together these advancements 1) allow us to visualize our constructs while they are still embedded, enabling in-process measurements of the as-printed geometry 2) open the possibility of using OCT to assess the quality of large bioprinted constructs such as human-scale

tissues and organs and 3) enable us to generate 3D reconstructions of the actual bioprinted construct for dimensional measurements, error detection, and to ensure that patient-specific geometries are accurately reproduced to provide high-quality evidence for regulatory agencies that FRESH is ready for the clinic.

Results

Integration of Optical Coherence Tomography into a High Performance Bioprinter

Previously we have reported developing open-source, low-cost bioprinters based off commercial plastic printers to lower the barrier to entry for the field and help drive innovation for regenerative medicine applications (*3*, *23*, *24*). The plastic printers on which these bioprinters are based have sufficient performance for a wide range of bioprinting applications (*1*–*3*, *25*); however, their positional accuracy is limited by their belt and pully driven configurations and is on the order of ±100 μm (*26*). For applications such as medical device fabrication and process validation, more advanced bioprinting platforms with higher accuracy are necessary.

To address this challenge, we designed a new high-performance bioprinter with a dedicated OCT scan head for in-process imaging and validation to ensure that the specifications of our bioprinter did not limit our printing capabilities (Fig. 1A and fig. S1). In addition to the OCT scan head, this bioprinter incorporates two of our Replistruder syringe pump extruders and utilizes a gantry configuration of four high-precision stages with positional accuracy of 8 microns over their full 100 mm travel (*27*). To assess our printing resolution and OCT imaging capabilities we developed a

benchmark model with both positive (regions of solid material) and negative (regions devoid of material) features covering three orders-of-magnitude from 10 mm down to 100 μm, and six open channels ranging from 500 μm down to 150 μm in width (Fig. 1B). This benchmark was imaged with the integrated OCT scan head during and after printing, and while embedded in the FRESH gelatin microparticle support bath (Fig. 1C) as well as in other media such as solidified gelatin and water. Before printing, the benchmark model must be sliced into layer-by-layer G-code instructions for our bioprinter to execute (Fig. 1D). The benchmark model was FRESH printed from a collagen type I and imaged via brightfield photography after melting and removal of the gelatin microparticle support bath (Fig. 1E). The G-code features (infill) and channels from Fig. 1D were qualitatively well recapitulated, with all channels visibly open.

Next, we evaluated the performance of the OCT imaging system with the FRESH printed benchmark model in either the FRESH gelatin microparticle support bath, melted and resolidified gelatin, or water. We began by capturing an OCT image of the benchmark model while it was still embedded in the highly light-scattering gelatin microparticle support bath (Fig. 1F). The outlines of larger features and the channels are visible, but the fidelity of the image is not sufficient for accurate measurement. To reduce the support bath opacity, we melted and resolidified the gelatin microparticles and captured another OCT image of the benchmark model (Fig. 1G). In this image more of the benchmark model's G-code features and the channel lumens can be clearly identified, but the signal decays sufficiently throughout the depth of the print that the bottom layers cannot be resolved. Finally, we removed the gelatin and captured an OCT image of the benchmark model while submerged in water (Fig. 1H). In this image all the channels and features of

the G-code are resolved throughout the depth of the print. A side-by-side comparison for the benchmark imaged in the support bath, resolidified gelatin, and water highlights the major scattering effects of the medium on the OCT quality (Supplementary Movie 1). To quantify the signal quality of the OCT images acquired in different media (Fig. 1, F to H) we utilized the signal to noise ratio (SNR) formula $SNR\ (dB) = 10\log_{10}\left(\left(\frac{\mu_{Sig}-\mu_{BG}}{\sigma_{BG}}\right)^2\right)$, where μ_{Sig} is the average of the signal, μ_{BG} is the average of the background, and σ_{BG} is the standard deviation of the background (*28*). This analysis shows a linear decay in SNR with an average 6.41 dB higher SNR in water compared to embedded in gelatin and an average 9.38 dB higher SNR in water compared to embedded in the gelatin microparticle support bath (Fig. 1I). Since the SNR of the benchmark imaged with OCT in water (Fig. 1H) was sufficiently high, we were able to measure all channel widths using a custom MATLAB image analysis script. The root mean squared (RMS) error of the measured width from the intended width for all channels was 12.52 μm and the Pearson correlation coefficient between measured and intended width was 0.9989 (Fig. 1J). In addition to measuring individual channels, the 3D nature of the OCT images allows us to use segmentation to build a 3D reconstruction of the printed benchmark model (Fig. 1K). The face-on and top-down views (right) show the infill pattern s well as the channels. The isometric view of the bottom layers (left) shows that the decay in SNR (Fig.1I) creates difficulties when segmenting the full print, resulting in an incomplete reconstruction. Together these data show the accuracy of our bioprinter and that OCT can be a useful tool for analyzing FRESH printed constructs, but that signal quality in the gelatin microparticle support bath must be significantly improved for in-process imaging.

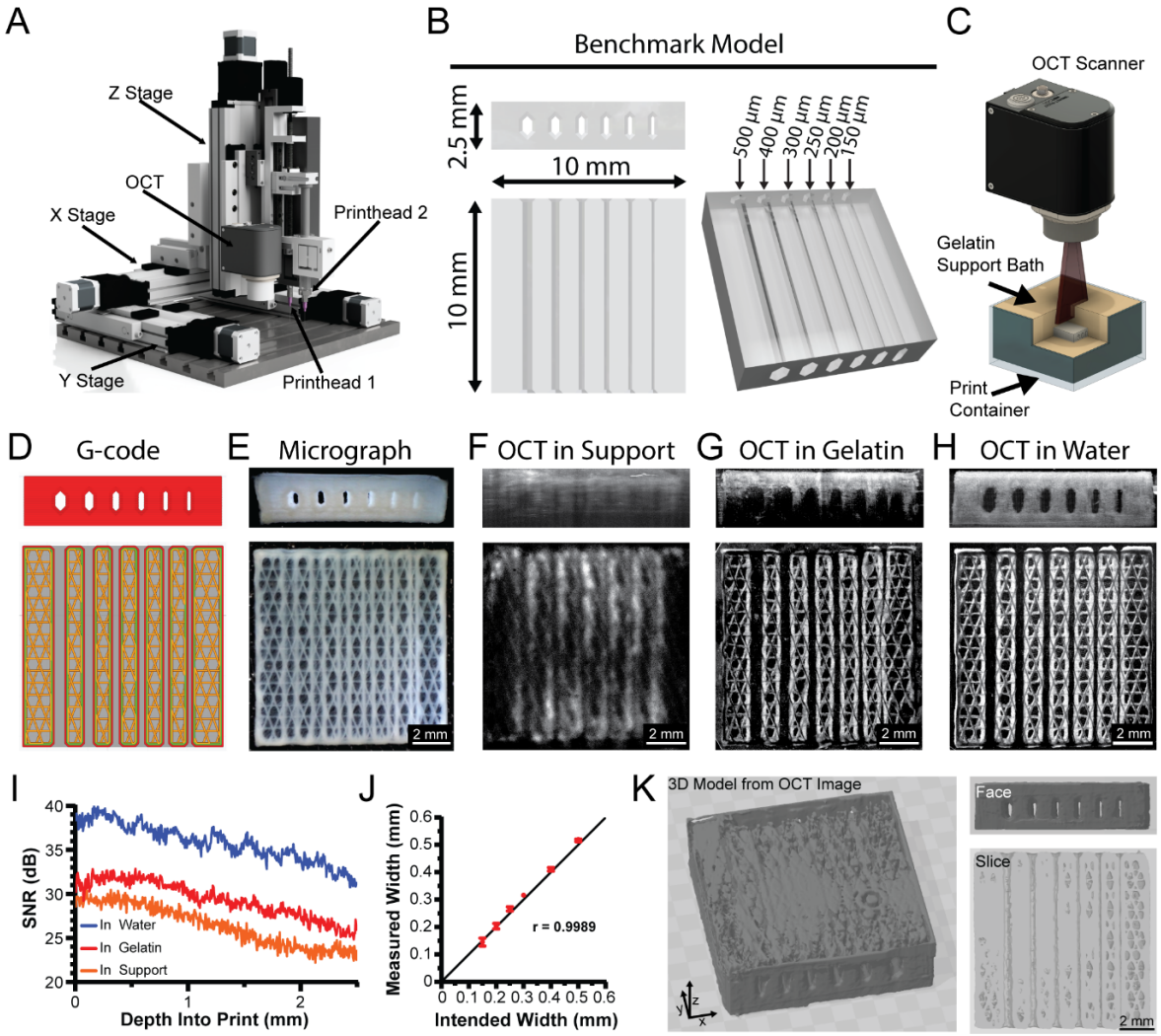

Figure 1| Design and integration of optical coherence tomography (OCT) into the FRESH printing platform. (**A**) 3D render of a custom-designed high-performance 3D bioprinter with dual extruders and an OCT scan head. (**B**) A benchmark model with internal channels of varying widths to test printer performance, resolution capabilities, and imaging quality. (**C**) Example rendering of OCT imaging of a FRESH printed construct within the gelatin microparticle support bath. (**D**) G-code 3D printer pathing of benchmark model channel cross section. (**E**) Photomicrograph of the benchmark model FRESH printed from collagen-I showing end on and top-down views. (**F-H**) OCT imaging of the benchmark model in the gelatin microparticle support bath, melted and resolidified gelatin, or water respectively. (**I**) Analysis of the OCT SNR for the collagen benchmark model within either gelatin microparticle support bath, melted and resolidified gelatin, or water. All three SNR curves are statistically significantly different from each other ($p<0.0001$, $n = 12$ total measurements from 3 benchmark prints each, Wilcoxon signed-rank test). (**J**) Correlation between the intended internal channel width and the measured width via OCT ($n = 4$, Pearson's correlation of $r = 0.9989$). (**K**) Images of the 3D OCT image data showing the full reconstruction, an end on view, and a cross-section through the internal channels.

Enhanced In-Process Image Quality with High Contrast Collagen and Sequential Imaging

OCT images acquired while printed objects are still embedded within the gelatin microparticle support bath (Fig. 1F) lack sufficient quality for in-process imaging and must be improved to a level comparable to submerged in water imaging to be useful. To increase the OCT signal and improve contrast we choose to incorporate a contrast agent, titanium dioxide (TiO_2), into our base collagen bioink (*29*). Specifically, we incorporated 250 parts per million (PPM) of TiO_2 into our collagen type I inks (high contrast collagen), which is a biologically safe concentration for drugs and medical devices according to the FDA (FDA e-CFR §73.1575, §73.3126). For comparison, we printed a benchmark model using our plain collagen and another with the high contrast collagen. We imaged the two benchmark models while still embedded at the end of printing (Fig. 2A). This revealed a clear qualitative difference in the imaging quality throughout the full depth. To quantify the signal improvement, we again calculated SNR for both printed benchmarks which showed an average 3.78 dB increase in SNR with the TiO2 added across all depths (Fig. 2B).

While increasing contrast of the collagen bioink improved SNR, we can also improve OCT image quality by decreasing the scattering and absorption of the gelatin microparticle support bath. One approach is to decrease the thickness of gelatin microparticle support bath that must be imaged through. To do this we printed the gelatin microparticle support bath using a second printhead (Fig. 2C), which filled the dish over time (Fig. 2D). Additionally, we developed a custom MATLAB code that interleaves the G-code for the gelatin microparticle support bath (Fig. 2E top) and the G-code for the

object to be printed (Fig. 2E bottom) to allow for printing within the printed gelatin microparticle support bath. In sequential steps, the gelatin microparticle support bath is first deposited (Fig. 2F left), then a section of the object is printed with high contrast collagen (Fig. 2F middle), and finally the OCT scan head is positioned over the print to acquire an image (Fig. 2F right). Throughout the printing process OCT image stacks of the printed object are acquired at evenly spaced z-height intervals (Supplementary Movie 2). All of the acquired OCT stacks are then registered in 3D and stitched together to form a complete composite OCT image stack.

Comparison of the OCT image acquired at the end of the print (single, Fig. 2G top) to the composite OCT image resulting from in process OCT imaging (composite, Fig. 2G bottom) shows a significant improvement in image signal quality, specifically as depth increases (Supplementary Movie 3) (*30*). By calculating the SNR at depth for the single and composite OCT images (Fig. 2H) we can see that for the composite the SNR no longer linearly decays and by 2 mm in depth the difference in SNR between the two images is up to 10.61 dB.

With the increase in SNR provided by high contrast collagen and enhanced OCT image quality due to in process imaging, we can quantitatively measure external and internal features of our prints such as the outer width (Fig. 2I red, 2J), the width of the inner walls (Fig. 2I gold, 2K), and the spacing between filaments (Fig. 2I blue, 2L). OCT images acquired after release confirm that printing the gelatin microparticle support bath did not affect the final printed dimensions, with no apparent change in print quality (fig. S2). These results, showing printing of micron scale features with minimal deviation from intended dimensions, demonstrate the high geometric precision and accuracy of our

bioprinter and FRESH printing process. They also demonstrate our ability to combine high contrast collagen I bioink, printing of FRESH gelatin microparticle support bath, and sequential OCT imaging for in-process 3D imaging and dimensional analysis.

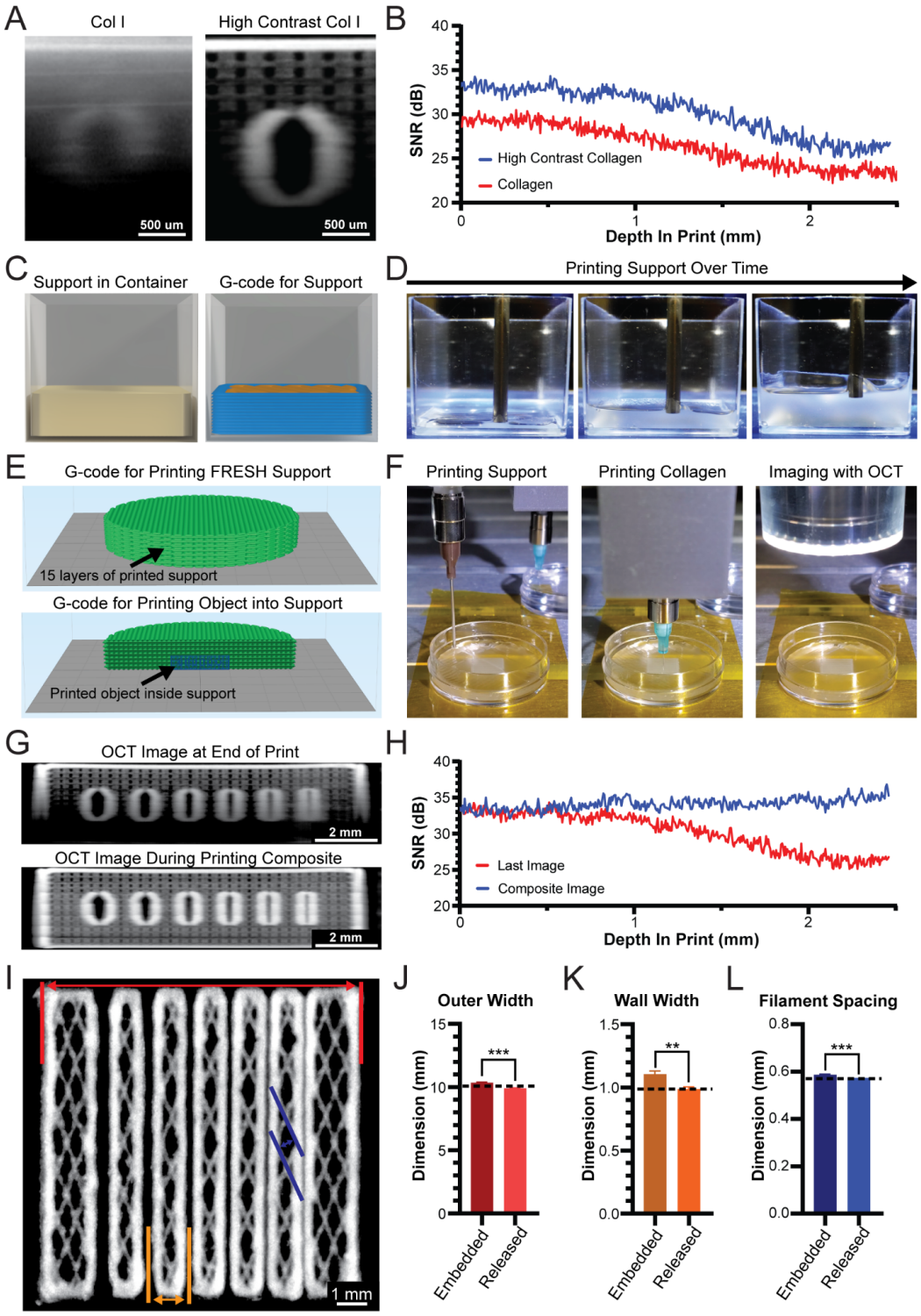

Figure 2| Development of a high contrast collagen bioink and printing of gelatin microparticle support bath to improve embedded OCT imaging (**A**) OCT image cross-section of benchmark model channel printed from collagen-I or high contrast collagen-I embedded in the FRESH gelatin microparticle support bath. (**B**) OCT SNR analysis for a collagen and high contrast collagen benchmark model within the gelatin microparticle support bath. The two SNR curves are statistically significantly different from each other ($p<0.0001$, n = 9 total measurements from 3 benchmark prints each, Wilcoxon signed-rank test). (**C**) 3D render of FRESH gelatin microparticle support bath within a print container (left) and layer-by-layer G-code (right). (**D**) Time-lapse images of gelatin microparticle support bath printing. (**E**) G-code for printing the gelatin microparticle support bath (top) and for printing an object inside of the gelatin microparticle support bath (bottom). (**F**) Stepwise process of printing the support bath, printing a collagen construct inside of the support bath, and OCT image acquisition. (**G**) OCT imaging performed at the end of the print (top) or intermittently during printing to produce a composite image (bottom). (**H**) OCT SNR for image acquired at the end of print (Last Image) or by compositing in-process OCT images. The two SNR curves are statistically significantly different from each other ($p<0.0001$, n = 9 total measurements from 3 benchmark prints each, Wilcoxon signed-rank test). (**I**) Composite OCT cross-section image for evaluation of print fidelity in terms of outer width (red), channel wall width (gold), and filament spacing (blue). (**J**) OCT measured outer width while the print was embedded in the gelatin microparticle support bath or following print release (mean ± STD.; n = 3 prints, measurement at every x linescan in yz stack, embedded vs. CAD $P = 0.0095$, Released vs. CAD $P = 0.0606$, Embedded vs. Released $P = 0.0004$ [***] by Student's two-tailed unpaired *t* test). Dashed line represents the 3D model expected value. (**K**) OCT measured wall width while the print was embedded in the gelatin microparticle support bath or following print release (mean ± STD.; n = 3 prints, highlighted wall measured at every x linescan in yz stack, embedded vs. CAD $P = 0.0179$, Released vs. CAD $P = 0.3448$, Embedded vs. Released $P = 0.0026$ [**] by Student's two-tailed unpaired *t* test). (**L**) OCT measured filament spacing while the print was embedded in the gelatin microparticle support bath or following print release (mean ± STD.; n = 3 prints, 12 filaments each, embedded vs. CAD $P = 0.0418$, Released vs. CAD $P = 0.0002$, Embedded vs. Released $P = 0.0008$ [***] by Student's two-tailed unpaired *t* test).

Increasing Transparency of Gelatin Microparticle Support Bath to Further Improve In-Process Image Quality

The opacity of the FRESH gelatin microparticle support bath has always made it challenging to visualize printed objects during the printing process, and to image prints while embedded. To solve this challenge and further improve OCT image quality, we sought to improve the transparency of the gelatin microparticle support bath by

decreasing the light scattering behavior. The majority of the opacity and light scattering for FRESH gelatin microparticles stems from a difference in the refractive indices (RI) of the gelatin microparticles themselves and the medium surrounding the particles. An effective approach to reduce this type of scattering and improve transparency is to match the RI of the surrounding media to the RI of the microparticles (Fig. 3A right) (*31*, *32*). Due to the FRESH gelatin microparticles inherent opacity when suspended in an aqueous buffer, we knew that the RI of the microparticles was likely higher than the RI of water (1.333). Therefore, we initially replaced the aqueous buffer with a higher RI biologically compatible solution called histopaque (a mixture of polysucrose and sodium diatrizoate). Ideally, as the RI of the surrounding media approaches the RI of the FRESH gelatin microparticles the transparency should increase. However, the RI of the highest concentration histopaque (1.367) commercially available was not sufficient to match the RI of the microparticles and only slightly improved transparency. To achieve a higher RI solution, we utilized high concentration polysucrose; however, at the higher concentrations necessary for RI > 1.367, the solution viscosity increased considerably, and was incompatible with the shear stress characteristics required for the FRESH gelatin microparticle support bath (*33*). Finally, we evaluated the other component of histopaque, sodium diatrizoate, which is an iodinated x-ray contrast agent. Instead of using sodium diatrizoate, which is not iso-osmolar, we chose a non-ionic, iso-osmolar contrast agent with high RI called iodixanol. Iodixanol is also cell and tissue safe, endotoxin free, and comes as a 60% solution in water at a RI of 1.429 (*34*).

To find the RI of the gelatin microparticles and achieve a transparent FRESH support bath we placed the gelatin microparticles within increasing concentrations of

iodixanol with RI ranging from 1.333 to 1.429 and captured phase contrast images. By analyzing the fringe boundaries of individual particles within these images (Fig. 3B left) we identified a minimum value, at which the RI of the microparticles and surrounding iodixanol solution are most closely matched (RI = 1.4083). Images of these particles at a RI below and above the identified RI of the particles (Fig. 3B right, top and bottom) show bright fringes, while at the particle RI (Fig. 3B right, middle) the particles and fringes are difficult to see (fig. S3). On a macroscale, when the gelatin microparticles are prepared for printing the difference is also visible between the plain support (Fig. 3C left), which is opaque and blocks the checkered background, and the clear support (Fig. 3C right), through which the checkered background can easily be seen. While the iodixanol improves clarity of the FRESH gelatin microparticle support bath at visible wavelengths it is essential to show that the clarity also improves OCT imaging depth and image quality (1300 nm light).

To evaluate OCT imaging performance in the clear gelatin microparticle support bath we 3D printed a plastic container with a sloping bottom that once filled allows us to image the bottom of the dish through increasing depths of support bath (Fig. 3D). When imaging through the plain gelatin microparticle support bath the image quality degrades after a few millimeters (~2-3 mm) and the deepest parts of the dish cannot be resolved (Fig. 3E). In contrast, when imaging through the clear gelatin microparticle support bath the image quality is improved, and the deepest part of the dish can be resolved well (Fig. 3F, Supplementary Movie 4). We quantified the differences in signal intensity between these two conditions (Fig. 3G). Both display an exponential decay, with the signal in the plain support decaying faster (k = 0.4135) than in the clear gelatin microparticle support

bath (k = 0.1709). To further characterize the clear gelatin microparticle support bath's improved transparency throughout the visible-IR wavelengths of light we performed an absorbance spectral analysis (Fig. 3H). There was an average decrease in absorption of 91.4 ± 2.3% (mean ± std) from plain to clear gelatin microparticle support bath. Finally, to determine the OCT SNR of our collagen I inks within the clear gelatin microparticle support bath we printed filaments (400 μm diameter) of plain collagen (Fig. 3I top) and high contrast collagen (Fig. 3I bottom). The high contrast collagen showed a significant increase in SNR compared to plain collagen (Fig. 3J). The combined increase in signal from the high contrast collagen and the improved transparency of the clear gelatin microparticle support bath now allows for the direct visualization of an embedded object during the printing process (Supplementary Movie 5). Together these data show that we can significantly improve the transparency of the gelatin microparticle support bath and the OCT image quality of embedded collagen constructs by reducing light scattering using a RI matching approach and adding a contrast agent to the collagen I bioink.

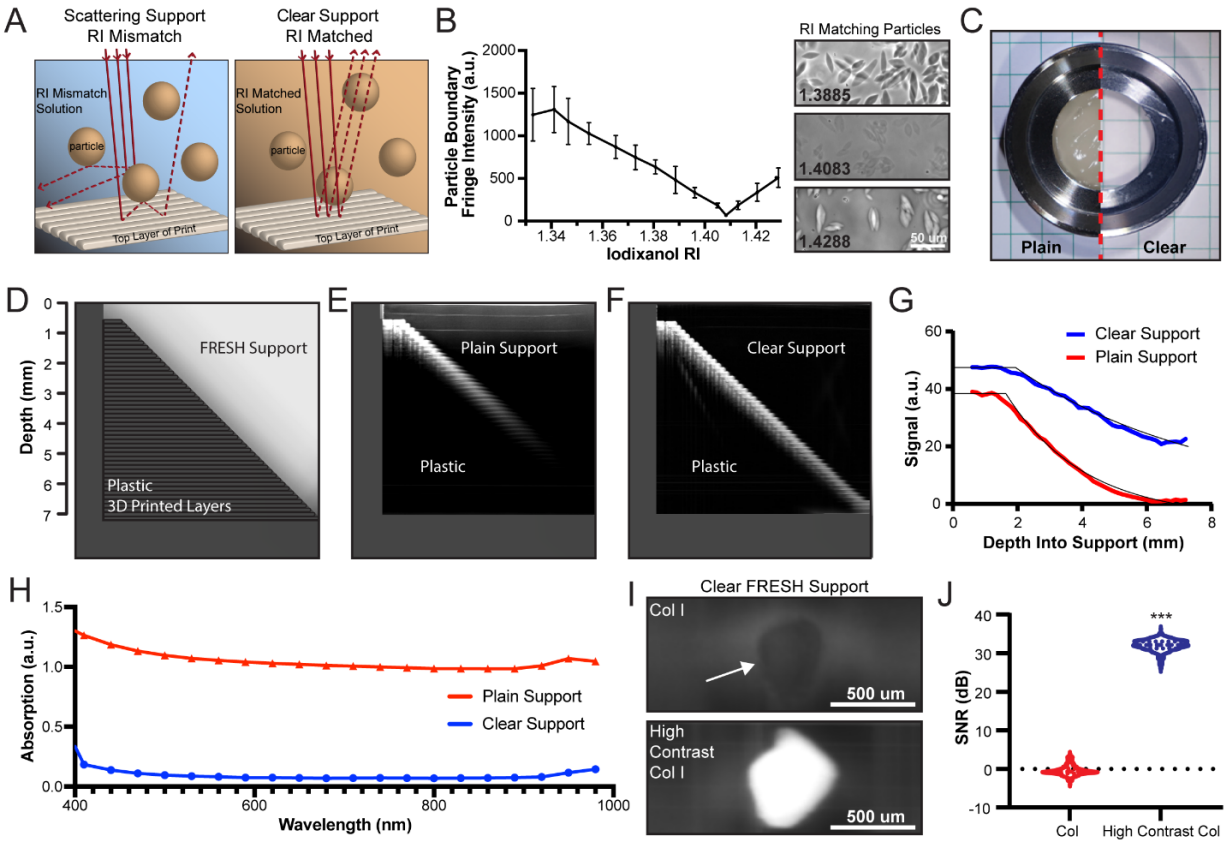

Figure 3| A transparent gelatin microparticle support bath increases OCT signal to noise and penetration depth. (**A**) For FRESH embedded printing, the gelatin microparticle support bath has an opaque appearance due to light scattering from the difference in RI between the particles and fluid phase solution. When the fluid phase RI matches the RI of the particles less light is scattered and absorbed which increases the gelatin microparticle support bath transparency. (**B**) Analysis of phase contrast imaging of gelatin microparticles' boundary fringe intensity in solutions of iodixanol. Example images of gelatin microparticles in iodixanol at the RI inflection point. (**C**) Plain (left) vs the "clear" (right) gelatin microparticle support bath. (**D**) Depiction of a sloping 3D printed plastic well designed to determine the OCT penetration depth through gelatin microparticle support bath by visualizing the printed layers throughout the well depth. (**E**) OCT image through plain gelatin microparticle support bath. (**F**) OCT image through clear gelatin microparticle support bath. (**G**) Exponential fit and analysis of OCT signal penetration depth for plain ($k = 0.4135$) and clear gelatin microparticle support baths ($k = 0.1709$). There is a significant difference between both curves at all depths ($p \leq 0.0003$, $n = 4$ containers each, two-way ANOVA with Tukey's multiple pair-wise comparisons). (**H**) Absorption spectra for plain vs. clear gelatin microparticle support baths. Both curves are significantly different at all wavelengths ($p < 0.0001$, n=6 wells, 2-way ANOVA with Tukey's multiple comparisons). (**I**) FRESH printed collagen-I (top) and high contrast collagen (Col)-I (bottom) filaments printed in clear gelatin microparticle support bath. (**J**) Analysis of the OCT SNR between collagen-I and high contrast collagen-I printed in clear gelatin microparticle support bath (mean ± STD.; n = 374 measurements along filament, $P < 0.0001$ [***] measured by Student's two-tailed unpaired *t* test).

In-Process Imaging and Quality Assessment of FRESH Printed Constructs

We next sought to demonstrate the combined impact of the clear gelatin microparticle support bath, high contrast collagen, and sequential OCT imaging. Our custom MATLAB code to generate G-code for support bath printing and in-process OCT imaging was adapted to utilize sequential OCT imaging during the printing process, without printing support. In a container pre-filled with clear gelatin microparticle support bath, several layers of the benchmark model were printed, then the OCT scan head was moved into position and the image was acquired; this process was repeated until the entire benchmark model was complete (Fig. 4A, Supplementary Movie 6). The images were composited (Fig. 4A bottom), which resulted in mitigation of the linear decay in SNR when only acquiring the OCT image at print completion (Fig. 4B). This recapitulates the results with high contrast collagen-I and printed plain gelatin microparticle support bath (Fig. 2H), but with substantially higher SNR values, resulting in further improved image quality. Additionally, we released the printed benchmark from the clear gelatin microparticle support bath and acquired OCT images to confirm that clearing with iodixanol did not affect the final printed dimensions or interfere with print release. The print released well and had no noticeable changes in terms of print quality or fidelity (fig. S4).

In terms of print validation, the combination of high contrast collagen and clear gelatin microparticle support bath allows us to not only measure the quality of our prints but also to detect errors. For example, we can identify internal void space errors, such as a bubble trapped in the top of a print (Fig. 4C). As most of the image below the bubble was captured before the bubble existed, the composite image does not show the bubble

casting a large shadow on features beneath it, as would be the case with a single image acquired at the end of a print. We can also detect over extrusion errors, such as the blockage of a channel (Fig. 4D). Due to the high SNR throughout the composite image we can utilize automatic image segmentation to produce a full 3D reconstruction of the printed object (Fig. 4E, fig. S5) (*35*). Using gauging software we compared the surfaces of two 3D meshes to measure deviations of the 3D reconstruction from the original 3D model, which for the benchmark model shown was an average of –20.9 ± 60.4 μm (Fig. 4E, fig. S5) (*36*). While this 3D reconstruction was built using OCT images captured sequentially, time-lapse OCT imaging while the construct is being printed is also possible (fig. S6, Supplementary Movie 7).

In addition to detecting simple defects, we can utilize in-process imaging to systematically identify deviations in printed objects that would result in a loss of function. To demonstrate this, we designed a 3D microfluidic mixing network, with features varying in all 3 axes and channels ranging in size from 0.5 to 1 mm within a collagen block (Fig. 4G). A photomicrograph of the mixing network 3D printed using high contrast collagen shows recapitulation of the intended geometry in a top-down view (Fig. 4H). To test our detection capabilities, we introduced a defect into the mixing network model that would block flow from one side of the network, rendering it non-functional (Fig. 4I, Supplementary Movie 8). After printing and imaging in the clear gelatin microparticle support bath we inverted the OCT images to extract the internal network shape and performed quantitative 3D gauging. Overall, the designed-defect mixing network showed an average deviation of –53.4 ± 62.1 μm, and clearly revealed the presence of the defect (Fig. 4J). By implementing a pass/fail criterion on the size of positive deviation we can

automate the detection of this defect (Fig. 4K). These data show that the combination of a clear gelatin microparticle support bath, high contrast collagen bioink, and sequential imaging provides a high SNR that makes possible in-process monitoring and 3D error detection in an embedded bioprinting approach.

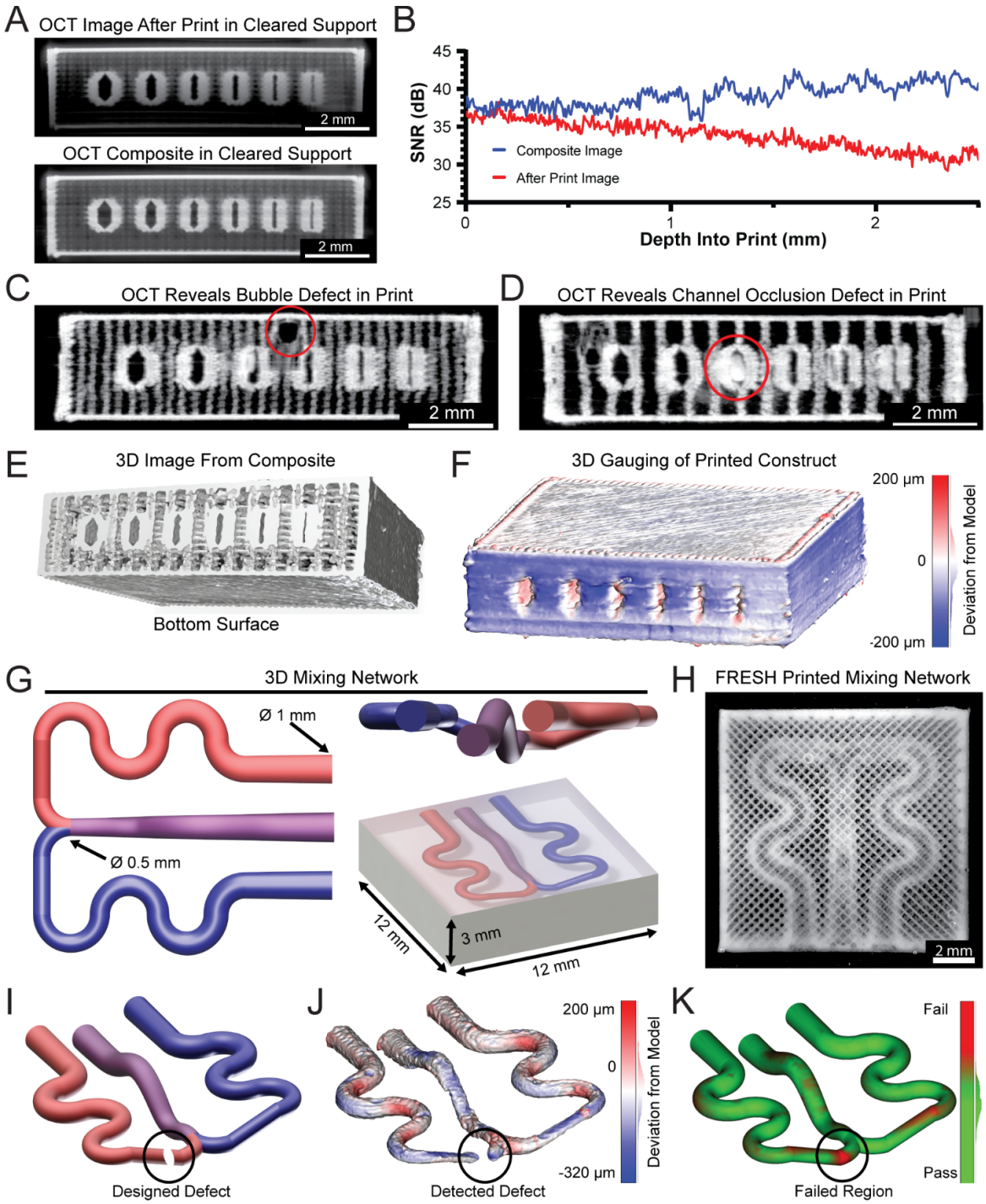

Figure 4| In-process OCT imaging and error detection of FRESH printed constructs. (**A**) Comparison of OCT imaging in clear gelatin microparticle support bath after print completion (top) or during in-process OCT imaging and composite image creation (bottom). (**B**) Analysis of OCT SNR after print imaging and during in-process imaging and composite image creation throughout the benchmark model depth. The two SNR curves are statistically significantly different from each other ($p<0.0001$, $n = 9$ total measurements from 3 benchmark prints each, Wilcoxon signed-rank test). (**C**) In-process OCT imaging reveals an internal print defect due to an introduced air bubble. (**D**) Unintentional channel occlusion detected by in-process OCT imaging. (**E**) 3D reconstruction using composite OCT image of a benchmark model. (**F**) Quantitative 3D gauging analysis to detect deviations in the reconstruction of the printed model compared to the computer-generated model. (**G**) 3D renders of a computer-generated mixing network to highlight FRESH printing and OCT capabilities. (**H**) Top-down view of a FRESH printed 3D mixing network from collagen-I. (**I**) An engineered defect was designed into the mixing network to mimic a blockage to test the OCT detection capabilities. (**J**) Quantitative 3D gauging analysis revealing a void at the location of the engineered defect. (**K**) A pass-fail deviation analysis was implemented to compare the printed and imaged 3D volume to the expected computer model for validation or rejection of the final printed construct.

In-Process Imaging and Dimensional Accuracy Analysis of Medical Imaging Derived Organic Models

For in-process imaging to be useful for transitioning FRESH printed constructs into clinical applications it must work well not only with simplified models such as the benchmark model and mixing network, but also with models derived from patient-specific medical imaging. To demonstrate this, we used our clear gelatin microparticle support bath and high contrast collagen to print and in-process image several such models. The first anatomic structure we printed was a segment of the vestibular apparatus from the inner ear (Fig. 5A, CAD Model). This shape inherently stress-tests the printing and imaging systems due to the patent semicircular canals oriented in three mutually orthogonal planes. The embedded print was clearly visible and showed good reproduction of the model including patency of the three semicircular canals (Fig. 5A, Embedded Print). The 3D OCT image composited from multiple images acquired during printing showed high

signal quality throughout the print depth (Fig. 5A, 3D OCT Image). This allowed us to generate a 3D surface which reveals both external and internal features, with inner channels approximately 325 μm in diameter (Fig. 5A, X-Ray Surface, Supplementary Movie 9). To evaluate the overall print fidelity, we performed gauging analysis which showed an average deviation of 17.8 ± 43.3 μm (Fig. 5A, Gauging Analysis). This small average deviation highlights the capabilities of our custom bioprinter and again demonstrates that FRESH printing with our clear gelatin microparticle support bath is not affected by the clearing process.

The second organic structure we printed was a segment of the circle of Willis, the arterial system of the brain (Fig. 5B, CAD Model). An unsupported patent vascular network, like this, would be challenging to 3D bioprint without FRESH and would be almost impossible to image in an aqueous solution or air. This model demonstrates our ability to print, image, and segment tortuous patent tubular structures with high-aspect-ratio (long and thin) and out of plane features (posterior cerebral arteries). The embedded print showed good visual reproduction of the model including the vertebral arteries, the anterior spinal artery, the middle cerebral arteries, and the posterior and anterior cerebral arteries (Fig. 5B, Embedded Print). The 3D OCT composite image had a high SNR and no decrease in signal throughout the depth of the print (Fig. 5B, 3D OCT Image). Automatic segmentation and 3D surface creation revealed the presence of both external and internal features, with the patent inner lumen of the right vertebral artery measuring approximately 450 μm in diameter (Fig. 5B, X-Ray Surface, Supplementary Movie 10). Gauging of the 3D surfaces compared to the original 3D CAD model created from medical imaging data showed a vascular network with an average deviation of 21.8 ± 53.2 μm

(Fig. 5B, Gauging Analysis). Our embedded imaging approach therefore allows for both the validation of print geometry and dimensions as well as the confirmation of a patent vascular network which is essential for perfusion applications.

The next organic structure we printed was the brainstem (Fig. 5C, CAD Model). This model is difficult to print due to the extremely small size of the cranial nerves (~250 μm in diameter) and their close proximity to each other (~200 μm center to center) as well as the subtle surface features on the thalami (~300 μm in depth). Visually, the embedded construct was easy to see and displayed good visual reproduction of the CAD model including the thalami, the midbrain, the pons, and the medulla (Fig. 5C, Embedded Print). The 3D OCT composited image again displayed high signal quality throughout the depth of the print with no apparent loss of signal (Fig. 5C, 3D OCT Image). The 3D surface model exhibited both external and internal features, though in this case the internal surface is just an offset shell from the external surface, as the actual brain stem is not hollow (Fig. 5C, X-Ray Surface, Supplementary Movie 11). Gauging of the 3D surfaces revealed reproduction of the cranial nerves and subtle surface features of the thalami with an overall average deviation of 21.4 ± 63.1 μm which is an order of magnitude below the smallest distinct feature within the model (Fig. 5C, Gauging Analysis).

The final organic structure we printed was a kidney (Fig. 5D, CAD Model). This structure showcased our ability to print and image complex internal structures (renal artery, renal vein, calyces, and ureter) within a larger construct (the whole kidney). While embedded, the print showed good visual reproduction of the CAD model with visible internal calyces as well as the renal artery, vein, and ureter (Fig. 5D, Embedded Print). The 3D OCT image composited from multiple in-process images showed a high SNR

throughout the depth of the print and even revealed the individual filaments that comprised the layers of the print (Fig. 5D, 3D OCT Image). The 3D OCT data was then segmented into a 3D surface which enhanced visualization of both external and internal features, including the open ureter, with an inner diameter of approximately 300 μm (Fig. 5D, X-Ray Surface, Supplementary Movie 12). Lastly, we evaluated the OCT performance and print fidelity via gauging analysis which revealed recapitulation of the complex internal structures and an average deviation of -23.8 ± 121.9 μm (Fig. 5D, Gauging Analysis). In all, the various organic tissues printed here highlight our ability to fabricate accurate ECM scaffolds from medical imaging data using FRESH bioprinting and demonstrate the high-resolution 3D imaging achieved using in-process OCT acquisition in combination with a high contrast collagen bioink and a clear gelatin microparticle support bath.

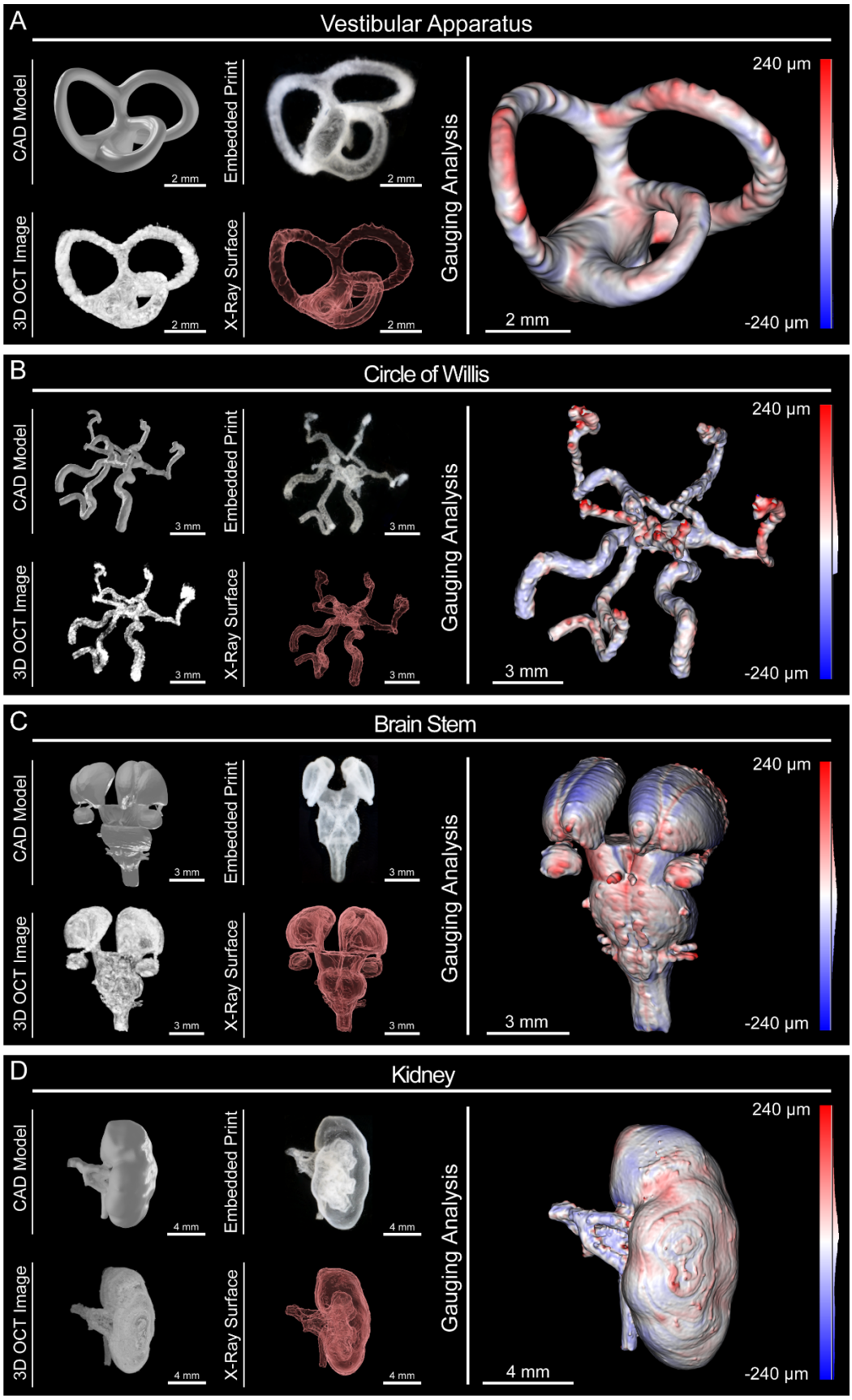
A
Vestibular Apparatus
CAD Model
Embedded Print
3D OCT Image
X-Ray Surface
Gauging Analysis
2 mm
240 µm
-240 µm
B
Circle of Willis
3 mm
C
Brain Stem
D
Kidney
4 mm

Figure 5| In-process OCT monitoring and 3D image reconstruction of medical imaging derived FRESH printed constructs. Four medical imaging derived models were chosen to demonstrate FRESH printing capabilities and OCT imaging using high contrast collagen in clear gelatin microparticle support bath. For each model we show five representations: 1) CAD model, 2) photograph of the embedded FRESH print in clear gelatin microparticle support bath, 3) an isometric view of the composite 3D OCT image, 4) an X-Ray view showing internal features, and 5) the results of quantitative gauging showing deviations of the 3D reconstruction from OCT imaging versus the computer model (red is oversized, blue is undersized). (**A**) Vestibular Apparatus with three orthogonal semicircular canals. (**B**) Circle of Willis showing vertebral arteries, anterior spinal artery, middle cerebral arteries, and posterior and anterior cerebral arteries. (**C**) Brain Stem with thalami, midbrain, pons, medulla and cranial nerves. (**D**) Kidney demonstrating internal calyces, ureter, and blood supply.

Discussion

As 3D bioprinting improves beyond simple linear stacking of hydrogels and into new applications that promise clinical utility, such as patient-specific scaffolds for surgical training, functional heart valves, perfusable vasculature, and contractile tissues, new manufacturing hurdles are arising that limit clinical translation. One long-standing challenge of bioprinting is the difficulty of monitoring the printing process and creating a complete 3D reconstruction for dimensional validation and error detection (*4*). If bioprinting is to be translated from the lab to the clinic, this limitation must be overcome to allow for the quality control required by regulators. For the FRESH gelatin microparticle support bath a significant limitation was its opacity due to significant scattering and absorption by the particles themselves (*1*, *2*). However, even with other transparent support baths (e.g. Carbopol), it has been difficult to find an appropriate imaging modality to monitor print quality (*37*, *38*). Many prints of interest have micron scale features, but overall dimensions on the order of tens of millimeters, which is a challenging range for many optical imaging techniques (*1–3*). Bright field imaging could allow for capture of the entire printed object in one acquisition and could easily be implemented into a 3D printing

platform but would not be able to provide the 3D information necessary to create a 3D reconstruction. Other imaging modalities such as reflectance or fluorescence confocal microscopy can provide sufficient resolution and optical sectioning for a high-resolution 3D reconstruction but would require long acquisition times due to smaller field of view and tile-scanning along with the computational complexity of combining many images into a single volumetric image. Additionally, implementation of these techniques for in-process imaging would require either the construction of a custom confocal microscope or a shuttle system to transfer samples between the printer and microscope. Finally, 3D imaging techniques designed for acquisition of larger volumes, such as μCT, while capable of providing sufficient resolution, require fixation, the incorporation of contrast agents, and embedding into an immobilization material as well as a long capture and reconstruction times that are not suitable for in-process imaging (*2*). Here we have demonstrated that optical coherence tomography combines the large imaging volumes (cubic centimeter) and high-resolution (~20 μm) capabilities of μCT, the optical sectioning of confocal imaging, and acquisition times (5 seconds up to 3 minutes) closer to bright field imaging to serve as an ideal in-process imaging tool for embedded 3D printing.

OCT also has the benefit of easy integration into a 3D bioprinter system. The commercially available scan heads are compact and light weight, with scanning mirrors, laser line and control inputs, and objective tightly packaged with height, width, and depth dimensions less than 10 cm. If the printing platform has sufficient space to mount this scan head, then incorporating OCT into a commercially available 3D bioprinter should be possible. Custom 3D bioprinters built using precision translation stages, such as the one we have presented here, provide easy mounting of the OCT scan head and the

repeatable positioning necessary (~8 μm) for sequential imaging as well as adequate printing speeds (up to 40 mm/s) with it attached (*27*). With different printer configurations it would also be possible to have a stationary OCT scan head, to which the sample was moved (allowing for custom, cutting-edge OCT systems), or beneath the sample for continuous live, in-process imaging (which we have demonstrated here).

In FRESH printing the similar RI of collagen and gelatin make them difficult to differentiate using OCT, as there is limited reflection at the boundary between the printed filaments and the gelatin microparticle support bath. The addition of TiO_2 as a contrast agent significantly improved the signal to noise ratio of our bioinks (*29*). While the addition of an exogenous contrast agent could affect the print characteristics of the bioink in some way, since the amount of TiO_2 added to our bioinks was so small, we did not notice any change in gelation or printability. Further, TiO_2 does not create a barrier for clinical translation and has the benefit of being classified by the FDA as bio-inert and safe for use in drugs and medical devices (FDA e-CFR §73.1575, §73.3126).

In addition to the incorporation of OCT and development of our high contrast collagen, we have demonstrated support printing with our dual material system, which is an adaptation of FRESH embedded printing with several benefits. All reports thus far of 3D bioprinting with the FRESH technique utilize pre-filled containers of support material, whether it is our gelatin microparticle support bath or some other support bath such as alginate. For applications where print dimensions are not too large (~5 mm tall), this works well. However, due to the limited length of finer gauge needle tips (34-gauge tips are a maximum of 6.35 mm long), printing taller constructs (>5 mm) at the highest resolution is not possible. We have previously overcome this limitation by building custom needle tips

with long, larger diameter barrels that are terminated in smaller diameter ends (*3*, *23*). However, when printing into deep dishes of gelatin microparticle support bath these tips tend to deflect distances that are incompatible with printing high-resolution constructs such as those we have presented here. By printing the gelatin microparticle support bath itself, we can minimize the deflection of the needle tip while now being able to print constructs of an arbitrary height (only limited by the printer travel). In addition to allowing for high-resolution printing of larger constructs, this makes OCT imaging of an embedded print possible, as the thickness of support that must be imaged through is minimal (a few hundred microns vs. millimeters). A potential limitation of this technique could be the volume of the gelatin microparticle support bath syringe. Here we utilized a 10 mL syringe for our gelatin microparticle support bath, but if a larger amount were necessary a syringe of increased volume could be adapted and possibly utilized in a different configuration (such as a Bowden setup utilizing a tube between the syringe and the needle tip) for support volumes up to 2 liters. Together, printing gelatin microparticle support bath and high contrast collagen provide new capabilities for FRESH printing while allowing for initial implementation of in-process imaging using OCT.

To improve embedded construct visibility and OCT image quality, we created a clear gelatin microparticle support bath using iodixanol, which has the added benefits of being cell safe, iso-osmolar, sterile and endotoxin tested (*34*). Changing the aqueous phase of the support could have affected the properties of our support bath that enable FRESH printing; however, we have shown that the quality of printed objects is not affected by the iodixanol either during printing or after melting the support away. The improved transparency in both the visible range and at the wavelength of our OCT system

allowed for direct visualization of FRESH printed collagen constructs during printing that were previously impossible to see until the gelatin microparticle support bath was removed. The transparent support bath is also amenable to bright field and fluorescence microscopy, which could be used for computer vision, to identify different bioink compositions, or for live cell imaging applications.

OCT imaging of bioprinted objects within our clear gelatin microparticle support bath provides a unique way to build a complete 3D reconstruction of the actual object in its printed form. Previously, it was necessary to first melt away the gelatin microparticle support bath and either submerge the construct in an aqueous solution or embed it in a clear hydrogel prior to capturing a 3D image. In both cases, small deviations in the construct shape and size occurred due to the soft deformable nature of the bioinks used in FRESH printed constructs. Now, by using the integrated OCT and compositing multiple image stacks acquired throughout the printing process we can create 3D reconstructions that enable us to directly gauge the actual printed object with the original digital model (*30*, *36*). This type of gauging is used extensively in subtractive manufacturing where coordinate measuring machines verify that the machined parts meet the required specifications (*39*). Our development of a clear gelatin microparticle support bath provides the opportunity to perform real-time gauging, as in subtractive manufacturing, to ensure the faithful reproduction of key dimensions that can be leveraged to alter our printing parameters to improve print quality. One limitation of our approach is the use of automatic segmentation in the reconstruction of our 3D models. Automatic segmentation is beneficial because it prevents bias from manual intervention, but it can influence the results depending on the image SNR and algorithm being utilized (*40*). Recently

developed machine learning based algorithms could be trained on bioprinted constructs to improve automatic segmentation and should provide higher accuracy when creating 3D reconstructions (*41*).

As bioprinting capabilities continue to improve towards functional organ constructs and transplantable medical devices there is an ever-growing need for an in-process monitoring and validation system to determine dimensional accuracy and detect potential print errors. In this manuscript we demonstrate the impact of integrating an OCT imaging system into a 3D bioprinter platform to perform in-process imaging of embedded bioprinted constructs. Additionally, the 3D bioprinter has dual extrusion capability which enables the printing of our gelatin microparticle support bath to improve OCT signal by reducing the amount of material that is imaged through. Combined with our newly developed high contrast collagen and leveraging the clear gelatin microparticle support bath we were able to print biologically-derived models (vestibular apparatus, circle of Willis, brainstem, and kidney, Fig. 5) and perform quantitative 3D gauging of their surfaces. In all cases we observed very minor average deviations (<50 μm) suggesting that our printing platform is both robust in fabrication and sensitive to micron scale error detection. This in-process imaging system can detect surface deviations, but those deviations can be utilized to perform pass fail error checking to identify features such as blocked channels, walls that are too thick or thin and regions with defects caused by bubbles or over extrusion of material. The reconstructions could also be utilized to determine whether the features of models are complete. For example, this would be useful in a microfluidic system where a hole could cause a leak or for a valve where fusion of the leaflets would block flow. These functional measures of print quality are more

important than simple deviation measurements and represent the type of quality control that will be necessary to comply with FDA and other regulatory agencies in the creation of clinically translatable bioprinted devices. In future work we intend to implement this in-process quality control in a fully automated fashion to provide routine analysis of printed constructs. In this way we will begin to develop a robust quality assurance program for bioprinted constructs to improve experimental success and to pave the way towards clinical translation for bioprinted tissues and medical devices.

Acknowledgments

Funding:

This work is supported by the Food & Drug Administration (R01FD006582), and the National Institutes of Health (F32HL142229, 1F30HL154728).

Author contributions:

All authors conceived the experiments and contributed to the scientific planning and discussions. J.W.T and D.J.S. prepared final figures and text. J.W.T conducted all bioprinting of constructs with in-process imaging. J.W.T and D.J.S. developed OCT imaging protocols and optical clearing protocols. J.W. T. wrote custom code in MATLAB for G-code editing. J. W.T and D. J. S performed image analysis in in FiJi and D.J.S. performed image analysis in Imaris. A.G. performed imaging and segmentation for creation of the kidney model. J.W.T, D.J.S., and A.W.F. wrote the paper and interpreted the data.

Competing interests:

A.W.F. has an equity stake in FluidForm Inc., which is a startup company commercializing FRESH 3D printing. FRESH 3D printing is the subject of patent protection including U.S. Patent 10,150,258 and provisional patent No. 63/082621. A.W.F. has an equity stake in Biolife4D Inc. and is a member of its scientific

Data and materials availability:

All digital models, for the Replistruder 5 as well as printed and reconstructed models, are available for download at Zenodo.org **(ADD WEBSITE LINK)**. Any raw data not presented in the main and supplemental text is available on request.

References:

1. T. J. Hinton, Q. Jallerat, R. N. Palchesko, J. H. Park, M. S. Grodzicki, H.-J. J. Shue, M. H. Ramadan, A. R. Hudson, A. W. Feinberg, Three-dimensional printing of complex biological structures by freeform reversible embedding of suspended hydrogels. *Science Advances*. **1**, e1500758–e1500758 (2015).

2. A. Lee, A. R. Hudson, D. J. Shiwarski, J. W. Tashman, T. J. Hinton, S. Yerneni, J. M. Bliley, P. G. Campbell, A. W. Feinberg, 3D bioprinting of collagen to rebuild components of the human heart. *Science*. **365**, 482–487 (2019).

3. E. Mirdamadi, J. W. Tashman, D. J. Shiwarski, R. N. Palchesko, A. W. Feinberg, FRESH 3D Bioprinting a Full-Size Model of the Human Heart. *ACS Biomaterials Science & Engineering*. **6**, 6453–6459 (2020).

4. D. J. Shiwarski, A. R. Hudson, J. W. Tashman, A. W. Feinberg, Emergence of FRESH 3D printing as a platform for advanced tissue biofabrication. *APL Bioengineering*. **5**, 010904 (2021).

5. N. Noor, A. Shapira, R. Edri, I. Gal, L. Wertheim, T. Dvir, Tissue Engineering: 3D Printing of Personalized Thick and Perfusable Cardiac Patches and Hearts (Adv. Sci. 11/2019). *Advanced Science*. **6**, 1970066 (2019).

6. M. A. Skylar-Scott, S. G. M. M. Uzel, L. L. Nam, J. H. Ahrens, R. L. Truby, S. Damaraju, J. A. Lewis, Biomanufacturing of organ-specific tissues with high cellular density and embedded vascular channels. *Sci Adv*. **5**, eaaw2459 (2019).

7. M. E. Kupfer, W.-H. H. Lin, V. Ravikumar, K. Qiu, L. Wang, L. Gao, D. B. Bhuiyan, M. Lenz, J. Ai, R. R. Mahutga, D. W. Townsend, J. Zhang, M. C. McAlpine, E. G. Tolkacheva, B. M. Ogle, In Situ Expansion, Differentiation, and Electromechanical Coupling of Human Cardiac Muscle in a 3D Bioprinted, Chambered Organoid. *Circulation Research*. **127**, 207–224 (2020).

8. S. Nuchitprasitchai, M. Roggemann, J. Pearce, *Three Hundred and Sixty Degree Real-Time Monitoring of 3-D Printing Using Computer Analysis of Two Camera Views* (2017), vol. 1.

9. A. Yasin Alibhai, C. Or, A. J. Witkin, Swept Source Optical Coherence Tomography: a Review. *Current Ophthalmology Reports*. **6**, 7–16 (2018).

10. J. Zhang, A. M. G. Sisley, A. J. Anderson, A. J. Taberner, C. N. J. McGhee, D. V. Patel, Characterization of a novel collagen scaffold for corneal tissue engineering. *Tissue Engineering - Part C: Methods*. **22**, 165–172 (2016).

11. M. L. Gabriele, G. Wollstein, H. Ishikawa, L. Kagemann, J. Xu, L. S. Folio, J. S. Schuman, Optical coherence tomography: History, current status, and laboratory work. *Investigative Ophthalmology and Visual Science*. **52**, 2425–2436 (2011).

12. J. G. Fujimoto, C. Pitris, S. A. Boppart, M. E. Brezinski, Optical Coherence Tomography: An Emerging Technology for Biomedical Imaging and Optical Biopsy. *Neoplasia*. **2**, 9–25 (2000).

13. S. S. Gao, Y. Jia, M. Zhang, J. P. Su, G. Liu, T. S. Hwang, S. T. Bailey, D. Huang, Optical coherence tomography angiography. *Investigative Ophthalmology and Visual Science*. **57**, OCT27–OCT36 (2016).

14. I. Laíns, J. C. Wang, Y. Cui, R. Katz, F. Vingopoulos, G. Staurenghi, D. G. Vavvas, J. W. Miller, J. B. Miller, Retinal applications of swept source optical coherence tomography (OCT) and optical coherence tomography angiography (OCTA). *Progress in Retinal and Eye Research*, 100951 (2021).

15. J. Czajkowski, T. Prykäri, E. Alarousu, J. Palosaari, R. Myllylä, Optical coherence tomography as a method of quality inspection for printed electronics products. *Optical Review*. **17**, 257–262 (2010).

16. E. Alarousu, A. AlSaggaf, G. E. Jabbour, Online monitoring of printed electronics by Spectral-Domain Optical Coherence Tomography. *Scientific Reports*. **3**, 1562 (2013).

17. L. Wang, M. Xu, L. Luo, Y. Zhou, P. Si, Iterative feedback bio-printing-derived cell-laden hydrogel scaffolds with optimal geometrical fidelity and cellular controllability. *Scientific Reports*. **8**, 2802 (2018).

18. A. Jannasch, C. Schnabel, R. Galli, S. Faak, P. Büttner, C. Dittfeld, S. M. Tugtekin, E. Koch, K. Matschke, Optical coherence tomography and multiphoton microscopy offer new options for the quantification of fibrotic aortic valve disease in ApoE−/− mice. *Scientific Reports*. **11**, 5834 (2021).

19. L. Wang, M. Xu, L. Zhang, Q. Zhou, L. Luo, Automated quantitative assessment of three-dimensional bioprinted hydrogel scaffolds using optical coherence tomography. *Biomedical Optics Express*. **7**, 894–910 (2016).

20. M. Martínez-Galdámez, J. Escartín, B. Pabón, C. Diaz, R. Martín-Reyes, A. Hermosín, E. Crespo, C. Rodríguez, G. Monedero, K. Joshi, D. K. Lopes, Optical coherence tomography: Translation from 3D-printed vascular models of the anterior cerebral circulation to the first human images of implanted surface modified flow diverters. *Interventional Neuroradiology*. **25**, 150–156 (2018).

21. J. Park, K. Lee, H. Kim, S. Park, R. E. Wijesinghe, J. Lee, S. Han, S. Lee, P. Kim, D. Cho, J. Jang, H. K. Kim, M. Jeon, J. Kim, Biocompatibility evaluation of bioprinted decellularized collagen sheet implanted in vivo cornea using swept-source optical coherence tomography. *Journal of Biophotonics*. **12**, e201900098 (2019).

22. C.-W. Chen, M. W. Betz, J. P. Fisher, A. Paek, Y. Chen, Macroporous Hydrogel Scaffolds and Their Characterization By Optical Coherence Tomography. *Tissue Engineering Part C: Methods*. **17**, 101–112 (2011).

23. K. Pusch, T. J. Hinton, A. W. Feinberg, Large volume syringe pump extruder for desktop 3D printers. *HardwareX*. **3**, 49–61 (2018).

24. J. W. Tashman, D. J. Shiwarski, A. W. Feinberg, A high performance open-source syringe extruder optimized for extrusion and retraction during FRESH 3D bioprinting. *HardwareX*. **9**, e00170 (2021).

25. S. M. Hull, C. D. Lindsay, L. G. Brunel, D. J. Shiwarski, J. W. Tashman, J. G. Roth, D. Myung, A. W. Feinberg, S. C. Heilshorn, 3D Bioprinting using UNIversal Orthogonal Network (UNION) Bioinks. *Advanced Functional Materials*. **n/a**, 2007983.

26. X. Wang, M. Jiang, Z. Zhou, J. Gou, D. Hui, 3D printing of polymer matrix composites: A review and prospective. *Composites Part B: Engineering*. **110**, 442–458 (2017).

27. 404 / 406XR Series Product Manual Electromechanical Positioning Systems (2004), pp. 1–49.

28. A. Agrawal, T. J. Pfefer, P. D. Woolliams, P. H. Tomlins, G. Nehmetallah, Methods to assess sensitivity of optical coherence tomography systems. *Biomedical Optics Express*. **8**, 902 (2017).

29. A. Kumar, I. Mondal, P. Roy, R. Poddar, TiO2 nanoparticles as exogenous contrast agent for 1 μm swept source optical coherence tomography: An in vitro study. *Laser Physics*. **28**, 035601 (2018).

30. S. Preibisch, S. Saalfeld, P. Tomancak, Globally optimal stitching of tiled 3D microscopic image acquisitions. *Bioinformatics*. **25**, 1463–1465 (2009).

31. R. Budwig, Refractive index matching methods for liquid flow investigations. *Experiments in Fluids*. **17**, 350–355 (1994).

32. J. Franklin, Z. Y. Wang, Refractive index matching: A general method for enhancing the optical clarity of a hydrogel matrix. *Chemistry of Materials*. **14**, 4487–4489 (2002).

33. Ficoll PM400 (2007), (available at https://us.vwr.com/assetsvc/asset/en_US/id/16286901/contents/17030005_data-file.pdf).

34. T. Boothe, L. Hilbert, M. Heide, L. Berninger, W. B. Huttner, V. Zaburdaev, N. L. Vastenhouw, E. W. Myers, D. N. Drechsel, J. C. Rink, A tunable refractive index

matching medium for live imaging cells, tissues and model organisms. *eLife*. **6**, 1–15 (2017).

35. A. Fedorov, R. Beichel, J. Kalpathy-Cramer, J. Finet, J. C. Fillion-Robin, S. Pujol, C. Bauer, D. Jennings, F. Fennessy, M. Sonka, J. Buatti, S. Aylward, J. V. Miller, S. Pieper, R. Kikinis, 3D Slicer as an image computing platform for the Quantitative Imaging Network. *Magnetic Resonance Imaging*. **30**, 1323–1341 (2012).

36. D. Girardeau-Montaut, Detection de changement sur des donnees geometriques tridimensionnelles. *Telecom Paris* (2006).

37. T. J. Hinton, A. Hudson, K. Pusch, A. Lee, A. W. Feinberg, 3D Printing PDMS Elastomer in a Hydrophilic Support Bath via Freeform Reversible Embedding. *ACS Biomater Sci Eng*. **2**, 1781–1786 (2016).

38. S. Abdollahi, A. Davis, J. H. Miller, A. W. Feinberg, Expert-guided optimization for 3D printing of soft and liquid materials. *PLoS One*. **13**, e0194890 (2018).

39. S. Y. Liang, R. L. Hecker, R. G. Landers, Machining process monitoring and control: The state-of-the-art. *Journal of Manufacturing Science and Engineering, Transactions of the ASME*. **126**, 297–310 (2004).

40. H. P. Narkhede, Review of Image Segmentation Techniques. *International Journal of Science and Modern Engineering*, 2319–6386 (2013).

41. C. Chen, C. Qin, H. Qiu, G. Tarroni, J. Duan, W. Bai, D. Rueckert, Deep learning for cardiac image segmentation: A review. *arXiv*. **7** (2019), doi:10.3389/fcvm.2020.00025.

Materials and Methods

Experimental Design:

The objectives of the experiments presented here were to develop the ability to perform in-process imaging of FRESH bioprinted constructs using optical coherence tomography. To improve signal to noise ratio and image quality using OCT we experimented with high contrast collagen inks, bioprinting the gelatin microparticle support bath, and refractive index matching to make the support transparent. We then demonstrated the effectiveness of these approaches by imaging functional and dimensional deviations of multiple bioprinted constructs including four that were derived from medical imaging data.

Integrated OCT Bioprinter:

The bioprinter used here was built using four Parker Hannefin 404XR 100 mm travel precision stages in a gantry configuration (8 μm travel accuracy verified using Mitutoyo absolute digimatic indicator 543-792, data not shown) mounted to an aluminum baseplate (www.worldofclamping.com) (27). The printer utilizes two custom Replistruder 5 syringe pumps built with high-precision metric leadscrews (www.McMaster.com) and compact Nema 11 motors with planetary gearsets (www.stepperonline.com); both were mounted to the Z stage. A dovetail adapter was designed, 3D printed from PLA plastic, and mounted to the Z stage to receive the OCT scanhead (Thorlabs), which was controlled with its own dedicated PC. The X, Y, and Z axes as well as the two extruders were controlled using a Duet 3 motion controller with a Raspberry Pi 4 single board computer dedicated for the user interface.

Plain FRESH Gelatin Microparticle Support Bath and Generation:

FRESH v2.0 gelatin microparticle support bathwas prepared as previously described using a complex coacervation method to produce gelatin microparticles (*2*). First, 2.0% (w/v) gelatin Type B (Fisher Chemical), 0.25% (w/v) Pluronic® F-127 (Sigma-Aldrich) and 0.1% (w/v) gum arabic (Sigma-Aldrich) were dissolved in a 50% (v/v) ethanol solution at 45ºC in a 1 L beaker and adjusted to 7.5 pH by addition of 1M hydrochloric acid (HCl). The beaker was then placed under an overhead stirrer (IKA, Model RW20), sealed with parafilm to minimize evaporation, and allowed to cool to room temperature while stirring overnight. The resulting gelatin microparticle support bath was transferred into 250 mL containers and centrifuged at 300 g for 2 min to compact the gelatin microparticles. The supernatant was removed and gelatin microparticles were resuspended in a 50% ethanol solution of 50 mM 4-(2-hydroxyethyl)-1-piperazineethanesulfonic acid (HEPES) (Corning) at pH 7.4, to remove the Pluronic® F-127. The gelatin microparticle support bath was then washed three times with the same Ethanol HEPES solution and stored until use at 4C. Prior to printing, the uncompacted support was centrifuged at 300 g for 2 minutes then washed with 50 mM HEPES and centrifuged at 750 g for 3 minutes a total of 4 additional times. After the last washing the gelatin microparticle support bath was again suspended in 50 mM HEPES and was degassed in a vacuum chamber for 15 min, followed by centrifugation at 1900-2100 g, depending on level of compaction desired, for 5 min. The supernatant was removed and the gelatin microparticle support bath was transferred into a print container.

Collagen Bioink Preparation:

All collagen bioinks were purchased as LifeInk 200 (Advanced Biomatrix). For bioprinting these inks were prepared as previously described (*2*). Briefly, 35 mg/mL LifeInk was mixed with syringes in a 2:1 ratio with .24M acetic acid to produce a 23.33 mg/mL acidified collagen ink. The ink was then centrifuged at 3000 g for 5 minutes to remove bubbles. To produce high contrast collagen inks an appropriate amount of 0.3-1.0 μm TiO_2 powder (Atlantic Equipment Engineers) was then weighed out for a 250 PPM mixture with the acidified collagen bioink. The TiO_2 powder was then dissolved in 100 μL of .24M acetic acid. This TiO_2 solution was then aspirated into the collagen through a needle. The TiO2 collagen mixture was then mixed 100 times between two syringes. The ink was then centrifuged at 3000 g for 5 minutes to remove bubbles. For printing the bioinks were transferred to a 500 μL gastight syringe (Hamilton Company).

OCT Imaging:

To acquire an image with the Thorlabs Vega 1300 nm OCT system (VEG210C1) the sample is first placed under the objective (OCT-LK4 objective). The system was started in the 2D mode with a scanline intersecting the sample. The sample's surface was then brought into focus and shifted using the reference stage to highlight the region of interest and to set further parameters. The amplification and reference intensity were then set to provide the highest signal without introducing image artifacts. The polarizing filters were then adjusted to optimize the signal intensity and minimize image artifacts. For a 2D image the averaging and z depth were then set, and the image was acquired at this point. For a 3D volume the mode was switched to 3D then the x, and y pixel dimensions were set to provide sufficient resolution while allowing for averaging and the amount of

averaging was set (typically 16.22 μm or 20 μm with 10 averages). Finally, the image was acquired. When utilizing the OCT mounted to the bioprinter for in-process imaging this same process was executed after the printer automatically positioned the scan head and paused for imaging. Acquired images were exported as 32-bit Tiff files for further processing.

Printing Both Bioink and Gelatin Microparticle Support Bath with In-Process Imaging:

To generate print pathing for multimaterial printing with in-process imaging we used a combination of open-source software and custom code. First the object to be printed and the volume of gelatin microparticle support bath to be printed were generated using Autodesk Inventor (Autodesk) or acquired from another source. These models were then loaded into Ultimaker Cura (Ultimaker) and processed into G-code using print parameters appropriate to the needle and syringe diameter being used. Next the G-codes were imported into a custom MATLAB script (Mathworks) designed to interleave the support print, the collagen print, and the imaging steps (meshGcode_OCTandSupport.m). The script takes advantage of the ability built into the Duet 3 implementation of G-code to store multiple toolhead positions. Using an index of the layer change comments in the G-code (automatically generated by Cura) the MATLAB script inserts small G-code scripts that use these toolhead positions to swap between extruder 1 (bioink), extruder 2 (gelatin microparticle support bath), and the OCT scan head. This custom script also allows for selection of the number of initial layers of gelatin microparticle support bath prior to initializing the collagen print and the number

of layers of collagen to print prior to a new layer of support. The OCT scan head is also automatically raised by the thickness of the new layers printed to maintain focus on them.

Prior to printing, the high contrast collagen bioink is centrifuged at 3000g for 5 minutes in a 10 mL plastic BD syringe and 450 µL is transferred to a 500 µL Hamilton gastight syringe. The plain gelatin microparticle support bath is centrifuged at 2000 g for 5 minutes in a 10 mL plastic BD syringe and is transferred to a 10 mL Hamilton gastight syringe. These inks, in their syringes, are loaded into their dedicated Replistruder 5 syringe pumps. Then, using the tip of the needle to measure the width and height, the first needle is aligned to the center of the print dish. For this first tool the origin is set using the G92 command. The first toolhead (T0) position is then set using the G10 command. Next, the second extruder's needle is centered on the dish and the position is again recorded using the G10 command, but for the second toolhead (T1). Finally, the OCT is aligned by centering its objective on the dish. Next the Z positions must be set. The first extruder (T0) is touched off to the bottom surface of the print dish and the G92 and G10 commands are used to set its Z offset. This process is repeated with the second extruder (T1) and the G10 command. Finally, the OCT is shifted in Z until the boundary at the bottom of the dish is in focus and the G10 command is used to set the offset of the focal plane. At this point the Duet 3 knows all the relative positions of the tools attached to the Z axis and is ready to print.

The second extruder (T1) is then returned to the center of the dish, using the measured offsets from the alignment process. Plastic dishes are filled with DI (for collagen bioink) or 50 mM HEPES (for support ink) and placed such that the inactive extruder needle is submerged (to prevent drying out and clogging). At this point the print

can be initiated by selecting the G-code on the Duet 3 interface. When the printer reaches the first pause for imaging the user can acquire an image using the Vega OCT's PC and then reinitiate printing using the Duet 3 interface.

Index of Refraction Measurement:

Index of refraction measurements for Iodixanol solutions were taken using a Hanna Instruments digital refractometer (HI96800). Briefly the refractometer was calibrated using deionized water, then the sample of interest was placed on the flint glass for measurement. The sample was allowed to equilibrate in temperature with the steel ring of the refractometer. Measurements were repeated until the 4th digit was consistent across measurements.

Identification of Gelatin Microparticle Support Bath Index of Refraction:

Plain gelatin microparticle support bath was prepared as described above. A high viscosity pipette was used to transfer 100 uL of compacted gelatin microparticle support bath into 2 mL of prepared Iodixanol solutions ranging from 0% to 60% in a 12 well plate. The support was then dispersed thoroughly within the Iodixanol solutions using clean pipette tips. Coverslips were used to trap the particles against the bottom of the well, which was necessary as Iodixanol solutions above 30% were denser than the gelatin microparticle support bath and floated the particles. Images were then acquired using a Nikon Eclipse TS100 microscope using a 20X phase objective and a Photometrics CoolSnapES camera run by MicroManager. The images were captured with identical exposure and illumination settings to allow for direct comparison.

The Iodixanol solutions were measured with our digital refractometer as described previously. To compare the particle clarity at different indices of refraction the peak to

trough difference of the high contrast phase boundary was quantified using a line scan analysis in FIJI ImageJ software for n = 13 particles in each image. Then the absolute value of this was plotted against the refractive index to identify the refractive index and iodixanol concentration that resulted in the clearest support solution.

Clear FRESH Gelatin Microparticle Support Bath Generation

To produce clear gelatin microparticle support bath using iodixanol the initial process is the same as plain support, described above except 250 mM HEPES is used instead of 50 mM HEPES. After the plain support is prepared for printing (e.g., centrifuged at 2000g for 5 minutes and supernatant removed), the supernatant is poured out and the remaining supernatant is absorbed with Kim wipes. The desired final concentration of Iodixanol ranged from 47.5% to 50% for optimal clarity and print characteristics, here we demonstrate bringing the concentration to 50%. First, Iodixanol reused from previous support preparations, at roughly 50%, is measured using our Hanna Instruments digital refractometer. The refractive index is utilized to determine the exact Iodixanol concentration. Sufficient Iodixanol is added to the support to bring the mass ratio of Iodixanol to 26% (mass ratio of 1:1.1 support:~50% Iodixanol). The solution is then vortexed. After mixing the 26% Iodixanol support is centrifuged at 3500 g for 5 minutes. After compaction, the Iodixanol supernatant is removed. At this point new 60% Iodixanol is added at a mass ratio sufficient to bring the final solution up to 50% Iodixanol (mass ratio of 1:2.3 support:60% Iodixanol). This 50% Iodixanol support solution is backfilled into capped 10 mL BD syringes (with plungers removed) and placed in a vacuum chamber for 15 minutes. The open barrel of the syringe was sealed with parafilm and then the syringes were centrifuged at 3500 g for 15 minutes. After centrifugation, the denser

Iodixanol is on the luer lock side of the syringe, covered by the compacted, clear gelatin microparticle support bath. A plunger is reintroduced into the backside of the syringe using a thin wire to allow for the passage of air. The Iodixanol solution is removed to another 10 mL BD syringe using a luer coupler and collected for later use in the first Iodixanol wash. After the Iodixanol has been removed, the clear gelatin microparticle support bath is collected into as few BD syringes as can hold the total volume. The support is transferred back and forth 50 times between these syringes to homogenize the mixture. Finally, the support is transferred to new 10 mL BD syringes with their plungers removed. The open barrel is covered with parafilm and the syringes are centrifuged at 3500g. The plungers are reinserted, again using a wire to break the seal, and the support is ready for use.

Absorbance Spectra Measurement:

To measure the absorbance of different gelatin microparticle support bath preparations we used a spectrophotometer (Molecular Devices SpectraMax i3x). For each preparation, an equal volume of gelatin microparticle support bath was deposited into the wells of a standard clear 24 well plate (thus producing an equal thickness). The spectrophotometer was set to acquire absorbance spectra from 230 nm to 980 nm in 30 nm steps for each filled well. The plastic dish absorbed light from 230 – 400 nm and so this range was excluded from the analysis. Measurements were taken at a consistent temperature of 24ºC.

Printing in Clear Gelatin Microparticle Support Bath with In-Process Imaging:

Generating print pathing for printing in clear gelatin microparticle support bath with in-process imaging is very similar to printing both the bioink and the support. Ultimaker Cura is utilized to generate the print pathing for the object to be printed. Next the G-code is imported into a custom MATLAB script (Mathworks) designed to interleave the collagen print and the imaging steps (meshGcode_OCT.m). The resulting G-code is uploaded to the Duet 3 printerboard via USB stick.

Prior to printing, the dish is filled with clear gelatin microparticle support bath and the top surface is scraped flat using a 20 mm x 20 mm square 1.5 coverslip. The top surface of the support is then covered in a layer of light mineral oil to prevent drying out (Fisher Scientific). Next the offset between the bioink toolhead (T0) and the OCT scan head (T2) is measured as previously described and stored using the G10 tool offset command. The bioink extruder (T0) is then returned to the center of the dish, using the measured offsets from the alignment process. A plastic dish is filled with DI (for collagen bioink) and placed such that the inactive extruder needle is submerged (to prevent drying out and clogging during imaging). At this point the print can be initiated by selecting the correct G-code on the Duet 3 interface. When the printer reaches the first pause for imaging the user can acquire an image using the Vega OCT's PC and then reinitiate printing using the Duet 3 interface.

Organic Model Creation

All models were created using Inventor Professional 2020 (Autodesk) or downloaded from online repositories. For the benchmark model and the 3D mixing model, the entire model was generated in Inventor then exported as an STL for printing. The vestibular apparatus was sourced from https://vestibularfirst.com/how-to-print-3d-

vestibular-apparatus/ and was derived from MRI data acquired by the University of Dundee School of Medicine (https://sketchfab.com/3d-models/anatomy-of-the-inner-ear-f80bda64666c4b8aaac8f63b7b82a0a0). The circle of Willis, derived from MRI data, was sourced from the NIH 3D Print Exchange (Model ID 3DPX-002604). The brain stem model, derived from MRI data, was sourced from the NIH 3D Print Exchange (Model ID 3DPX-003892). The kidney model was sourced from the University of Pittsburgh School of Medicine.

Image Analysis

To assess signal to noise ratio in OCT images they were first opened in FIJI ImageJ. Then areas of the image with high signal and adjacent areas of background were sampled. The resulting averages and standard deviations for each area were utilized in the equation $SNR\ (dB) = 10\log\left(\left(\frac{\mu_{Sig}-\mu_{BG}}{\sigma_{BG}}\right)^2\right)$ to calculate the signal to noise ratio, where μ_{Sig} is the average of the signal, μ_{BG} is the average of the background, and σ_{BG} is the standard deviation of the background (*28*).

To assess the signal intensity at different depths in plain and clear gelatin microparticle support bath a plastic dish was created with a sloped bottom that allowed for imaging through increasing depths of gelatin microparticle support bath. Images of the bottom of the dish were acquired using plain and clear gelatin microparticle support bath at the same imaging settings. Images were opened in FIJI and converted to 16-bit TIFFs using the same range of intensity values prior to conversion. The images were scaled to match each other, then regions of the same size were sampled at equivalent depths in each image. The resulting averages were utilized to create a curve of intensity at depth for plain and clear gelatin microparticle support bath.

To assess the quality of the printed resolution test object the acquired OCT images were opened in FIJI. The images were corrected for rotation about the x, y, and z axes. Cropped views of the middle 50% along the channel axis and 25% perpendicular to it were extracted from the images. These images were then 3D-median filtered with a 5-pixel filter width. The background intensity in the center of the channel was measured and used to perform background subtraction. The images were then automatically thresholded. The images were cropped to only include the channels and their walls. These stacks were saved and then imported into a custom MATLAB script that measured the width of the channel at each row in each slice of the segmented images and reported the average value of this width for all slices.

OCT Image Composites

To combine multiple OCT image stacks acquired throughout printing into a single composite image the pairwise stitching plugin was used in FIJI ImageJ with subpixel accuracy and linear gradient or maximum intensity fusion options set (*30*). First the raw images were rotated to orient the print to the pixel x, y, and z axes. Next the images were cropped to include the full last layer and the bottom of the print. These images were then resliced to a view perpendicular to the Z axis. The first stitching was performed with the first and second captured OCT stacks. The second stack was cropped to have approximately 10% overlap with the first. Overlapping regions of interest were highlighted to aid the plugin in registration. In subsequent stitching steps the same process was repeated but using the previously stitched image and the next stack to be incorporated, until the last stack was incorporated.

Gauging

To perform quantitative gauging of printed objects using the OCT images a full model of the printed object needed to be extracted. To do this the OCT images, either one acquired at the end of printing or a composite of multiple acquired throughout printing, were loaded into FIJI (NIH). These stacks were then filtered using the 3D-Median filter with a filter width of 3 pixels. The background subtraction tool was then used to remove background if necessary. The images were then converted into 16-bit tiffs and the histogram equalization was used. Local automatic thresholding was utilized to isolate the image data, using the savola method. Next erroneous spots were removed using the outlier removal tool. Finally, the segmented image stack was exported as a tiff.

The tiff was imported into 3D Slicer (http://www.slicer.org/). The integrated segmentation tools were used to isolate the print. The segmentation was manually edited to remove artifacts and islands and was then smoothed using a median filter with a 3 pixel width. After smoothing the reconstruction was exported as an STL file using the built-in exporter, taking care to set the pixel size to match the known pixel dimensions from OCT acquisition.

The reconstruction was loaded into 3D builder (Microsoft), where scaling was verified, and the mesh was simplified to aid with future processing. After saving the simplified mesh the reconstructed object was loaded, along with the digital model STL (which was used to generate the G-code for printing the object) into CloudCompare (http://www.cloudcompare.org/) (*36*). Using built in tools the two objects were oriented relative to each other, registered, then surface deviations were

calculated. This information was exported as false color images as well as mean and standard deviation.

3D Visualization in Imaris

We used Imaris (Bitplane, 9.5.1) for 3D rendering of the raw OCT data. The TIF file from the OCT data for each organic model was imported into Imaris. A surface object was created using the surface wizard function with local background subtraction and filtered using the “quality” filter to remove small non-specific objects. A mask of the surface object was created to act as a passthrough filter for the original OCT data to remove non-specific background from the 3D image. 3D renders of the background removed OCT data and the X-ray view of the surface object were exported as TIF images. Built in animation functionality was then used to make movies showing the internal features and highlighting internal complexity within the printed objects.

Statistics and Data Analysis

Statistical and graphical analyses were performed using Prism 9 (GraphPad) software and Excel (Microsoft v16). Statistical tests were chosen based on the experimental sample size, distribution, and data requirements. For comparison of SNR between benchmark models in plain gelatin microparticle support bath, gelatin, and water Wilcoxon paired signed-rank tests were used (Fig. 1I). For analysis of measured width of a benchmark imaged in water the Pearson correlation coefficient was calculated (Fig. 1J). For comparison of SNR between benchmark models in plain support using plain and high contrast collagen Wilcoxon paired signed-rank tests were used (Fig. 2B). For comparison of SNR between last image and composite image of benchmark models in plain support using high contrast collagen Wilcoxon paired signed-rank tests were used

(Fig. 2H). For comparison of embedded and released dimensions of benchmarks printed in plain support Student's two-tailed unpaired t test was used (Fig. 2 J to L). For comparison of OCT signal in plain and clear gelatin microparticle support bath at all depths 2-way ANOVA with Tukey's multiple comparisons was used (Fig. 3G). For comparison of absorbance in plain and clear gelatin microparticle support bath at all depths 2-way ANOVA with Tukey's multiple comparisons was used (Fig. 3H). For comparison of SNR of plain collagen and high contrast collagen in clear gelatin microparticle support bath Student's two-tailed unpaired t test was used (Fig. 3J). For comparison of SNR between last image and composite image of benchmark models in clear gelatin microparticle support bath using high contrast collagen Wilcoxon paired signed-rank tests were used (Fig. 4B). For analysis of measured width of a benchmark printed in printed support after release the Pearson correlation coefficient was calculated (fig. S2B). For analysis of measured width of a benchmark printed in clear gelatin microparticle support bath after release the Pearson correlation coefficient was calculated (fig. S4B). Preparation of figures and visuals was completed in Adobe Photoshop and Illustrator CS6 and CC. OCT images were edited in Fiji (ImageJ NIH) and Imaris 9.5.1 (Bitplane). 3D Reconstruction of OCT images was completed using 3D Slicer (http://www.slicer.org/). Gauging was accomplished using CloudCompare (http://www.cloudcompare.org/). Advanced image analysis and quantification was performed in MATLAB (Mathworks).